Constitutive equation for time independent plasticity and creep of 316 stainless steel at 550 °C

DOI:
10.1016/S0308-0161(03)00027-9

Available online at www.sciencedirect.com
SCIENCE DIRECT®
International Journal of Pressure Vessels and Piping 80 (2003) 97–109
INTERNATIONAL JOURNAL OF Pressure Vessels and Piping
www.elsevier.com/locate/ijpvp

Constitutive equations for time independent plasticity and creep of 316 stainless steel at 550 °C

D.R. Hayhurst*, F. Vakili-Tahami, J.Q. Zhou

Department of Mechanical, Aerospace and Manufacturing Engineering, UMIST, P.O. Box 88, Sackville Street, Manchester M60 1QD, UK

Received 5 August 1999; revised 23 January 2003; accepted 23 January 2003

Abstract

The paper concerns the development of constitutive equations for 316 stainless steel at 550 °C; it, firstly, considers time independent plastic straining at high temperature; and, secondly, describes how mechanisms-based creep constitutive equations have been formulated. It is shown how a power-law hardening model may be used to describe the effects of prior plastic pre-strain, by providing excellent comparisons with the results of experiments. The paper then develops constitutive equations for time dependent creep based on the theory of continuum damage mechanics. The corresponding state variable rate equations have been selected to include a description of strain hardening in primary creep, a major contributor to strain in this material, and also softening due to creep constrained cavity growth. Despite the paucity of data at lower stresses, corresponding to lifetimes in the region of 10^5 h, a model has been formulated which gives good predictions of experimental results over a wide stress range. The paper discusses how the time independent and time dependent models may be combined in a finite element analysis code to predict inelastic straining due to initial loading and to stress redistribution encountered in reheat cracking of welded pressure vessels.

Keywords: High-temperature creep; Continuum damage mechanics; Finite element method; Time-independent plasticity and creep; Creep damage; Austenitic stainless steel AISI 316; Uni-axial constitutive equations

1. Introduction

1.1. Reheat cracking

Cracks found in 316H stainless steel components in advanced gas cooled reactors have been identified as Reheat Cracking, caused by the accumulation of creep damage and creep strain due to the relaxation of weld-induced residual stresses. Holt [1] has performed finite element calculations to determine weld residual stresses, and hence study reheat crack initiation. Bradford [2] has also used finite element modelling to study reheat crack initiation in austenitic weldments. However, there have been few attempts to theoretically model the creep behaviour of Type 316 or 316H stainless steels, and from these models study the initiation and growth of reheat cracking. The continuum damage mechanics (CDM)-based analytical approach may be used to predict the location and initiation times of reheat cracks. Most importantly, the technique can be used to investigate if reheat cracking is limited to the crack initiation zone (crack arrest) or whether it extends beyond the initiation zone and leads to crack growth and failure, driven by the redistribution of post-weld residual stresses. In the latter case creep crack growth rates need to be predicted to assess safe-lifetimes.

CDM-based modelling [3–5] has been successfully used to predict creep crack growth using finite element-based numerical methods. However, it is necessary to identify a set of mechanisms-based CDM constitutive equations and to calibrate them using high-quality uni-axial and multi-axial time independent plasticity and creep tests data.

Welded pressure vessels operate for long periods of time, often in excess of 10^5 h; and, since reheat cracking is driven by the relaxation of post-weld residual stresses from values in excess of the yield stress to relatively low values, both long-term and short-term creep data, and the associated constitutive equations are required. These are needed both to interpolate and extrapolate the data, and for use in design

* Corresponding author. Tel.: +44-161-200-3817; fax: +44-161-200-4166.
E-mail address: d.r.hayhurst@umist.ac.uk (D.R. Hayhurst).

0308-0161/03/$ - see front matter © 2003 Elsevier Science Ltd. All rights reserved.
doi:10.1016/S0308-0161(03)00027-9

and component analysis. This paper concerns the behaviour of welded 316 stainless steel vessels operated at 550 °C.

1.2. Materials modelling and data requirements

The data available for short-term creep behaviour tend to be of a higher quality than that for longer term tests. This is due to the fact that long-term tests were initiated often up to 10 years ago; and, to the rapid technological development which has taken place in testing techniques. Long-term data are often lacking in details regarding initial loading of tests, and often tests have been interrupted many times to measure creep strain. Another complication in the testing of 316 stainless steel at 550 °C is that time independent plastic straining can take place not only on initial loading, but also during the creep test. The effects of the latter are to necessitate the use of true stress, rather than engineering stresses in any analytical work. In addition, good models are required to describe time independent plasticity to enable the decoupling of time independent plastic and time dependent creep strains. This aspect will be treated at length in the subsequent sections.

In this paper a set of mechanisms-based constitutive equations will be developed to describe the creep behaviour of the 316 stainless steel at 550 °C. The model considers both time independent plastic straining and time dependent creep. The approach adopted in this paper is not intended to be a general procedure for the development of CDM-models for combined time independent plasticity and time dependent creep. However, it relates to the development of constitutive equations for a Heysham I superheater header. The CDM constitutive equations have been used in another paper [6] to carry out a full reheat crack initiation and growth assessment of the Heysham I vessel. The supporting uni-axial creep test dataset has a significant amount of scatter associated with it. Despite this scatter the method produces a set of constitutive equations which give a good fit to the creep strain, minimum creep strain rate and rupture time over a wide range of stress, whilst describing creep ductility as a function of stress level.

The sources of experimental data which have been used to calibrate the constitutive equations sets are discussed in Section 2.

2. Sources of experimental data

A large database is available from the uni-axial creep tests performed by ERA [7], on material casts of Type 316 and 316H stainless steels at 550 °C. This is supplemented by tests carried out by British Energy [8,9] on Type 316H from the ex-Heysham I superheater header. These two data sources will be used exclusively to calibrate the constitutive models reported in this paper. Fortunately, the high stress datasets cover both time independent plasticity and time dependent creep.

Table 1
Cast origin of the available experimental data

Stress level	Initial engineering stress (MPa)	Origin	Code	Source
High	320	Ex-Heysham I superheater header	1D1/4	British energy
	300	Ex-Heysham I superheater header	1B2/4	British energy
	280	Ex-Heysham I superheater header	1B2/4	British energy
Low	232	ERA Cast	CQ	ERA
	201	ERA Cast	ACJ	ERA
	170	ERA Cast	BK	ERA

The cast origin of the datasets is summarised in Table 1. The data have been categorised into high stress and low stress groups. Since the available datasets contain a number of sub-populations or casts, statistical precautions are required in their treatment.

2.1. Cast dependency of data

Austenitic stainless steel 316 has a strong cast dependency both for the yield stress and for the creep properties. Since the creep tests used in this paper [7–9] have been carried out on different casts of materials, very wide scatter bands can be observed in the reported data. Hence, it is statistically inaccurate to obtain an overall trend-curve or behaviour without checking it with the individual trend-curves obtained for at least one of the well-represented casts [10]. Otherwise, there is a likelihood of erroneous selection due to the over-presentation of strong and/or weak casts. These features become apparent from a preliminary examination of the stress-lifetime and stress-minimum creep strain rate data for all the available test data. Hence, the need for a good correlation has been used as a procedure for the selection of representative test data. In addition, it is surprising that when this is done, groups of tests which relate to a particular stress range contain data originating from different batches of material. In the absence of more data which enables detailed characterisation of the different batches, this feature is seen as an attribute of the approach.

Due to the significant stress redistribution in reheat cracking problems, the stresses change from a very high level (well above the first yield stress) to very low stress levels commensurate with lifetimes in excess of 10^5 h. Therefore, the CDM-based model should be based on creep tests with a very wide range of stress level. To overcome this difficulty two approaches can be taken.

The ideal solution is to carry out a series of time independent plasticity and time dependent creep tests for each individual cast which cover a wide range of stress level. Then, develop a CDM-based model for each individual cast of material. Clearly, this solution is not

practical: firstly, such a sophisticated materials data bank is not available; and, secondly, the application of a single-cast-based CDM model to study the creep behaviour of another cast of material would cause significant error.

An alternative approach, which has been adopted in this paper, is to collect all the available data for different casts of material which cover a wide range of stress level, and which are pertinent to the materials used in model header tests or in-service plant. Then, identify a general trend which describes the creep behaviour for all casts of material. Based on this general trend, a set of representative data can be selected at each stress level for which tests have been carried out (six stress levels in this study). These datasets may be used to calibrate the constitutive equations set. In this way, a general CDM-based model will be developed which may be used in conjunction with finite element analysis methods to study the reheat cracking of the welded pressure vessels, regardless of their cast origin. However, the representative datasets may be associated with different casts of materials, and therefore, the quality of fit might be poor for one of the casts depending on the cast-characteristics of the material. The approach adopted in this paper addresses this shortcoming as follows.

(i) The available data [7–9] have been checked and classified and only well-represented datasets have been used in this paper. Hence, the risk of over representation of a strong or a weak cast has been minimised.

(ii) Due to the significant stress redistribution in reheat cracking problems, priority has been given to fitting data involving several casts over a wider range of stress level, rather than modelling the individual behaviour of a cast.

(iii) Based on the guidance given by British Standard PD6605 [10], the predicted creep behaviour has been checked against at least one well-represented cast to check if the predicted general trend is in parallel with the well-represented cast behaviour. In this spirit, the predicted creep properties have been compared with the experimental data associated with the selected representative datasets and a good agreement has been obtained. However, the predicted trend has not been checked against any individual cast data. To address this shortcoming, and to identify the cast dependency of the CDM-based model, the model will subsequently be used in CDM finite element analyses of reheat cracking of a welded pressure vessel which involves a series of sensitivity studies aimed at determining the effect of the variation of each creep property on the predicted vessel behaviour. In this way, the importance of cast to cast variations on material parameters will be assessed, at the component level, on reheat cracking behaviour.

2.2. Modelling of time independent plasticity and creep

Against the background presented in Section 2.1, the approach adopted in this paper to select a set of representative test results is summarised as follows.

(i) Review all available creep data for 316 stainless steel at 550 °C which relate to the material used to fabricate the welded pressure vessels which will be investigated in a future study of reheat cracking.

(ii) Select tests which are consistent and reliable in terms of initial plastic straining, minimum creep rates, rupture lifetimes and creep ductility.

(iii) Divide the available test data into two groups: short-term and long-term data. Identify the tests for which details are available for the initial loading and the subsequent creep deformation. For the high stress group, the loading data (stress–strain curves) and the creep test data are available; however, for the low stress group, no loading data are available, and only a few data points are available for each creep test. Hence, a power-law model has been developed to predict the initial plastic strain at low stress levels.

(iv) Select those datasets which correlate well with the rupture and minimum creep strain rate behaviour predicted by the CDM-based hyperbolic-sine constitutive equations. In other words, the data which show an approximate linear variation in both stress-logarithm of lifetime and stress-logarithm of minimum, creep strain rate plots. For this purpose, a graph has been produced which includes all the available experimental data and shows the variation of the initial engineering stress-logarithm of the lifetime. The reason for the selection of initial engineering stress and lifetime is twofold. Firstly, these values have been recorded for all tests. Secondly, they can be measured directly and their use causes minimum error. Having produced the graph showing the variation of the initial engineering stress with logarithm of the lifetime, a line has been fitted to all available test points using the least square method. Then, the closest points to this line have been selected at each stress level for which tests have been carried out (six stress levels in this study). These points represent the selected tests both at high stress and at low stress levels. Due to the approach adopted, the selected datasets also represent mean values, determined by the best least square line fitted to all experimental data in the initial engineering stress-logarithm of lifetime graph.

(v) Use the selected datasets to calibrate physically based constitutive equations. The latter is a pre-requisite for accurate CDM analysis of reheat cracking.

It is also worth reiterating that no attempt has been made to differentiate or categorise the available experimental data on a cast to cast base. It is recognised that the creep behaviour of 316 stainless steel may vary from one cast to another; however, the major desire is to develop a CDM model which is based on the correlated sets of experimental data independent of their cast origin. The implications of variations in the resulting constitutive parameters upon reheat cracking behaviour which arises from cast to cast variations have been studied by Vakili-Tahami and Hayhurst [6].

The following section addresses the development of the power-law model to describe the time independent plastic stress–strain behaviour. Then, the paper addresses the selection of the experimental data and calibration of the CDM-based constitutive equations for creep deformation and damage evolution to be used in a CDM-based finite element analysis code.

3. Time independent plastic stress–strain curve

Deformation of a structure usually consists of elastic, plastic and creep strains. To analyse the behaviour of structures, it is necessary to separate time independent plastic and time dependent (creep) components of strain; and to formulate constitutive equations for both of these conditions. To obtain material constants for creep constitutive equations, it is necessary to remove the initial strain and the accumulated time independent plastic strain from the total strain measured in creep tests under constant loading. To do this, a constitutive equation is required to describe the time independent or plastic true stress–true strain curve.

A power-law formulation has been used to model time independent plastic straining. It is important to emphasise that the power-law model has been used to describe the time independent plastic stress–strain curve only; and, a separate CDM-based constitutive equations set will be outlined in the later sections to describe time dependent creep behaviour.

3.1. Power-law model for stress–strain behaviour of virgin material

The power-law model for uni-axial conditions is

$$\varepsilon^{t} = (\sigma/E) + A_1(\sigma - \sigma_{yp})^{m}\delta(\sigma_{yp}), \tag{1}$$

where $\delta(\sigma_{yp}) = 0$ for $\sigma < \sigma_{yp}$; and, $\delta(\sigma_{yp}) = 1$ for $\sigma \geq \sigma_{yp}$, σ and σ_{yp} are stress and initial-yield stress, ε^{t} is total strain, E is Young's modulus, A_1 and m are material constants.

3.2. Fitting the model to the experimental data

The Young's modulus, E, and initial yield stress, σ_{yp}, can easily be obtained from uni-axial experimental data. To obtain the material constants; A_1 and m, an optimisation scheme has been used. The optimisation functional has been defined as follows

$$\phi_1 = \sum_{i=1}^{a}\left\{\sum_{j=1}^{b_i}(\varepsilon_j^{the} - \varepsilon_j^{exp})^2\right\}, \tag{2}$$

where a is the number of stress–strain curves, b_i is the number of data points on curve i, ε^{the} and ε^{exp} are the theoretical/predicted and experimental strains, respectively. The theoretical strains, ε^{the}, have been obtained using Eq. (1). The experimental strains, ε^{exp}, have been obtained using the test results provided by British Energy [8] showing the plastic behaviour of stainless steel 316 at high temperatures including 550 °C. Although these data are for different casts of material, they have been used in this study in the absence of more directly traceable data.

Table 2
Material constants derived by the minimisation of the optimisation functional (2) and Eq. (1)

E (MPa)	σ_{yp} (MPa)	A_1 (MPa)$^{-m}$	m
1.2263×10^5	90.1	0.3171×10^{-4}	1.494

3.3. Summary of results

The derived material constants are given in Table 2 and the predicted results are compared with the experimental data in Fig. 1. From Fig. 1, it is clear that there is a good agreement between the experimental data and the predicted values obtained using the power-law constitutive model.

3.4. Model for the stress–strain behaviour of pre-strained material

The effect of pre-straining in 316 stainless steel is, like in most other metals, mainly a type of isotropic hardening. In this section, the stress–strain behaviour of pre-strained material (5%) is studied. Since the initial plastic pre-straining has been carried out at room temperature, the pre-strained material has been modelled as a new material, for which the power-law equation is valid using the new material constants and new initial-yield stress

$$\varepsilon^{t} = (\sigma/E) + A_1^{*}(\sigma - \sigma_{yp}^{*})^{m^{*}}\delta(\sigma_{yp}^{*}), \tag{3}$$

where A_1^{*} and m^{*} are new material constants; and, σ_{yp}^{*} is the initial-yield stress. Following the same procedure discussed in the last sub-section, the new material constants have been obtained and presented in Table 3.

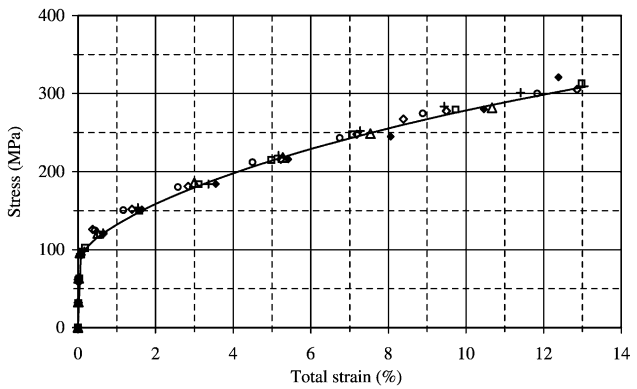

Fig. 1. Comparison of the experimental stress–strain data, symbols, with the predicted behaviour, solid line, obtained using power-law equation (1).

Table 3
Material constants for pre-strained material with $\varepsilon_{pre} = 5\%$ derived by the minimisation of the optimisation functional (2) and Eq. (3)

E (MPa)	σ^*_{yp} (MPa)	A^*_1 (MPa)$^{-m^*}$	m^*
1.2263×10^5	214.13	0.5968×10^{-4}	1.468

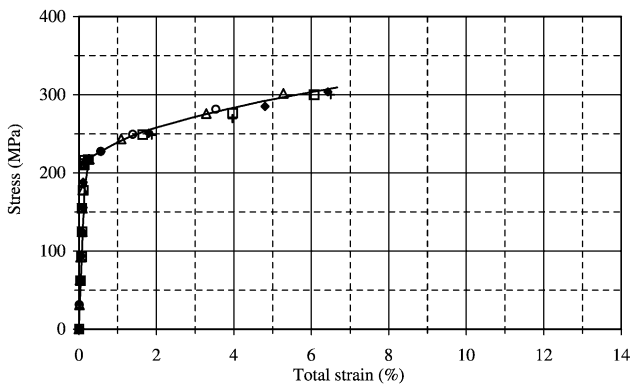

Fig. 2. Comparison of the experimental stress–strain curves, symbols, with the predicted behaviour, solid line, obtained using power-law equation (3) for pre-strained material with $\varepsilon_{pre} = 5\%$.

Fig. 2 shows the predicted results obtained using Eq. (3) and the experimental data [8] for the material which is pre-strained to $\varepsilon_{pre} = 5\%$. The figure shows that the predicted results agree very well with the experimental data.

3.5. Discussion of results

Firstly, the predicted results for the virgin material are compared with those for the pre-strained material with $\varepsilon_{pre} = 5\%$. The predicted stress–strain curves are shown in Fig. 3 with a 5% strain shift for the pre-strained material curve. The units given in Fig. 3 are those of true stress and engineering strain. The figure also shows the definition of the terms ε_{pre} and $\hat{\sigma}_{yp}$ which are plastic pre-strain and the corresponding modified initial-yield stress of material, respectively. It can be seen that the modified initial-yield stress, $\hat{\sigma}_{yp}$, is the stress level for the intersection between pre-strain elastic line and the plastic strain curve for the virgin material.

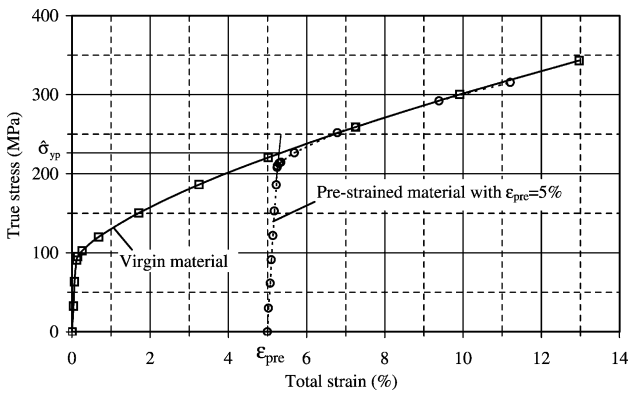

Fig. 3. Comparison of the predicted stress–strain curves for virgin material, solid line, and plastically pre-strained material with $\varepsilon_{pre} = 5\%$, broken line. The figure also shows the definition of the modified initial yield stress, $\hat{\sigma}_{yp}$, which is the stress level for the intersection of elastic line for the pre-strained material and the plastic curve for the virgin material.

From the figure, it is clear that the two curves are almost coincident when $\sigma \geq \hat{\sigma}_{yp}$ except that there is a marginal difference in the region of $\sigma^*_{yp} < \sigma \leq \hat{\sigma}_{yp}$. This comparison gives a good indication that the power-law model for the virgin material can also be used to model the stress–strain behaviour of pre-strained material by ignoring the marginal differences in the region of $\sigma^*_{yp} < \sigma \leq \hat{\sigma}_{yp}$ and by assuming an elastic response when $\sigma \leq \hat{\sigma}_{yp}$. In other words, the power-law model for virgin material can easily be modified to describe the stress–strain behaviour of both virgin and pre-strained materials. The modified model is given by

$$\varepsilon^t = (\sigma/E) + [A_1(\sigma - \sigma_{yp})^m - \varepsilon_{pre}]\delta(\hat{\sigma}_{yp}), \quad (4)$$

where E, σ_{yp}, A_1 and m are material constants for virgin material given in Table 2.

The modified initial-yield stress, $\hat{\sigma}_{yp}$ and plastic pre-strain, ε_{pre}, can easily be obtained using the stress–strain curve for the virgin material shown in Fig. 3. Hence, when the material constants for the virgin material together with the values of $\hat{\sigma}_{yp}$ and ε_{pre} are known, Eq. (4) can be used for the corresponding pre-strained material.

4. Uni-axial creep data

As discussed in Sections 1 and 2, to treat the available experimental data, it is necessary to carry out an analysis of the experimental data, and to choose a number of representative datasets from all ranges of the stress levels. The uni-axial creep data are taken from the tests performed by ERA [7] and British Energy [8,9] for Type 316 and 316H stainless steel and ex-Heysham I superheater header type 316H. The tests have been carried out at constant load and cover the temperature range of 500–700 °C and a stress range of 160–320 MPa. The test temperature of 550 °C has been selected since it coincides with the in-service temperature level at which reheat cracking has been investigated using the constitutive equations [6]. Spindler [11] has also given a summary of the available creep test results for Type 316 and 316H stainless steel and ex-Heysham I superheater header type 316H.

The scheme used to select the representative datasets has been discussed in Sections 1 and 2. This section discusses some of the main features of the creep data, such as lifetime, minimum strain rate and strain at failure, which play important roles in choosing representative data. These data are discussed in the following sections.

4.1. Rupture data

Firstly, the rupture data have been examined. Fig. 4 shows the variation of the initial engineering stress with logarithm of lifetime. All the available experimental data are shown in this figure using open circles. Initial engineering stress is defined as the applied constant load divided by the initial area of the testpiece cross-section. It is clear from the figure that lifetimes increase as the stress reduces. Fig. 4 also shows that the scatter in the data extends over a relatively wide stress range; the reason for this is possibly due to the different casts of material, different testing procedure at different laboratories and different heat treatment prior to creep testing [12].

Fig. 4 has been used to select the representative test data. This figure shows the variation of the initial engineering stress and lifetime. Since the selected datasets should correlate well with the rupture and minimum strain rate behaviour predicted by the CDM-based hyperbolic-sine constitutive equations, they are expected to show an approximate linear variation in both stress-logarithm of lifetime and stress-logarithm of minimum creep strain rate plots. To select the datasets, which satisfy the above condition, a line, shown as broken line in Fig. 4, has been obtained using the method discussed in Section 2.2(iv). In this way, six representative points have been selected which are shown as square and triangular symbols in Fig. 4 for high and low stress levels, respectively. It should be pointed out that none of the selected datasets are from the pre-strained data. Fig. 4 shows that the solid line, which is the best least square fit to the six selected data points, is very close to the broken line which is the mean value for all data points. However, it should be re-emphasised that the solid line has been obtained using the best fit to the six selected data points and no attempt has been made to average the experimental data points.

The selected datasets have been used to obtain the material constants in an optimisation procedure to be outlined later.

4.2. Minimum creep strain rate data

Fig. 5 shows all the available experimental data, denoted by open circles, for minimum creep strain rate. The data in this figure are plotted on axes of logarithm of minimum creep strain rate against initial engineering stress. The square and triangular symbols represent the selected test data which have been chosen based on the scheme explained in Sections 2 and 4.1 using Fig. 4. The solid line is the best least square fit to the six selected data points. From the figure, it can be seen that the minimum strain rate increases with the initial engineering stress; and that there is an approximate linear relationship between the logarithm of minimum creep strain rate and initial engineering stress.

Similarly, the scatter on experimental data extends over a relatively wide range of stress. Possible reasons for this are heat treatment, pre-straining [12] and different casts of material [11].

4.3. Creep strain at failure

Variation of engineering creep strain at failure, defined by total strain less initial loading strain, with initial engineering stress is given in Fig. 6. All the available experimental data are shown in this figure using open circles. The square and triangular symbols represent the selected test data which have been chosen based on the scheme explained in Sections 2 and 4.1 using Fig. 4. From Fig. 6, it can be seen that the data-scatter extends over a wide range of strain, and that the strains at failure change with initial stress and reach their lowest value in the region of initial stress $\sigma \geq 300$ MPa. Spindler [11] has carried out

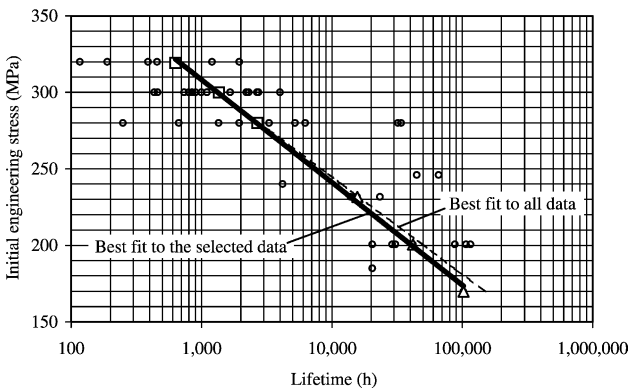

Fig. 4. Variation of the lifetime with initial engineering stress for uni-axial creep data for AISI 316 at 550 °C. The circles denote the available experimental data. The square and triangular symbols denote the selected test results for high stress and low stress levels, respectively. The solid line is the best fit to the selected experimental data; and, the broken line is the best fit to all the experimental data.

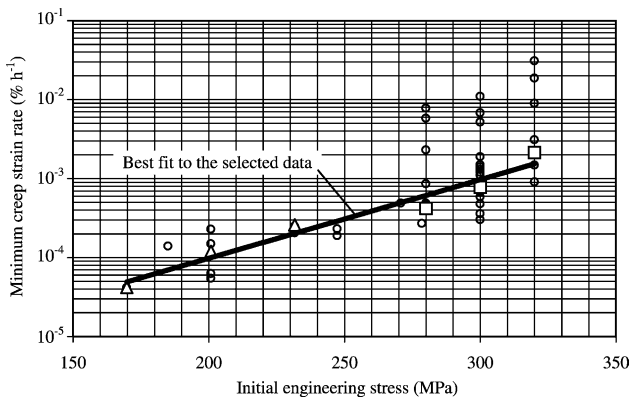

Fig. 5. Variation of the minimum creep strain rate with initial engineering stress for uni-axial creep data for AISI 316 at 550 °C. The circles denote the available experimental data. The square and triangular symbols denote the selected test results for high stress and low stress levels, respectively, which have been chosen using Fig. 4. The solid line is the best fit to the selected experimental data.

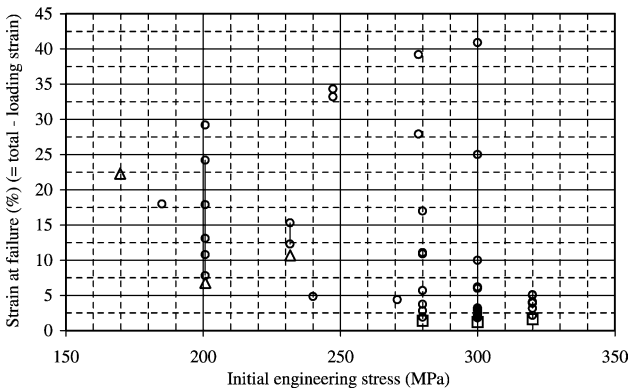

Fig. 6. Variation of the engineering strain at failure (= total strain-loading strain) with initial engineering stress for uni-axial creep data for AISI 316 at 550 °C. The circles denote the available experimental data. The square and triangular symbols denote the selected test results for high stress and low stress levels, respectively, which have been chosen using Fig. 4.

research on creep ductility of 316 stainless steel over a temperature range of between 500 and 700 °C. His work also shows that strain at failure usually scatters over a wide range and changes with stress. The work of Henderson et al. [13] reveals a similar conclusion. Furthermore, their research results show that at 550 °C the strain at failure reaches its lowest value in the region $\sigma = 300$ MPa.

The reason for the wide scatter of experimental data, shown in Fig. 6, is possibly due to the heat treatment carried out before creep testing, pre-straining [12] and different casts of material [11].

It is worth reiterating that 316 stainless steel is a highly creep resistant material at 550 °C; and, to achieve failure lifetimes of the order of 10^5 h, it is necessary to apply stresses above the initial plastic yield stress. Since the plastic stress–strain behaviour of the material shows modest strain hardening at 550 °C (Figs. 1 and 2), time independent plastic straining takes place not only in the initial loading but also during subsequent creep. The latter is due to the finite straining of the component; and, to the elevation of the true stress above the current yield stress. Although, the creep experimental data presented in Figs. 4–6 do not include the initial plastic strain, $\varepsilon^{\text{init}}$, they all included time independent plastic straining, ε^{tip}, which accumulates during constant load creep tests. This makes it necessary to take into account both the effects of initial plastic straining, $\varepsilon^{\text{init}}$, and of the accumulated time independent plastic straining, ε^{tip}, in the creep analyses of engineering components. The procedure used to decouple time independent plastic straining and creep strain will be outlined in the following sections.

5. CDM-based creep constitutive equations

CDM-based constitutive equations are used to predict creep rupture lifetime of 316 stainless steel. Physically based constitutive equations provide a description of the creep strain rate, incorporating the effects of changes in the microstructure due to creep damage mechanisms.

In the following sub-sections, the physically based CDM model and the constitutive equations will be discussed in detail.

5.1. The physically based model

To develop a set of CDM-based constitutive equations which describes the time independent plastic and time dependent creep straining of AISI 316 stainless steel a number of factors need to be taken into account [12]. These are:

1. The low strain hardening nature of the stress–strain curve, and hence the ability to produce large plastic stains for relatively small changes in stress.
2. The effect of plastic pre-strain on subsequent creep behaviour.
3. Strain hardening attributed to primary creep.
4. Material softening or creep damage due to intergranular cavitation.
5. The susceptibility of the dislocations to thermal recovery and of the carbides to coarsen, and their subsequent effect on creep deformation and failure.
6. The effects of multi-axial states of stress on creep ductility.

In the approach reported here a simplified model has been adopted, mainly because of the paucity of good quality data available at the low stresses encountered in operational plant. The approach separates the time dependent and time independent components of strain, and constitutive equations are developed for each mechanism separately.

In summary, the CDM-based model incorporates strain hardening attributed to primary creep and material softening due to nucleation controlled creep constrained cavity growth. The ageing mechanism has not been considered in this model. Since this paper addresses uni-axial behaviour only, the important effects of multi-axiality have not been considered here. However, this has been studied in detail by Vakili-Tahami and Hayhurst [6] in an investigation on reheat cracking in welded pressure vessels.

5.2. Constitutive equations for 316 stainless steel at 550 °C

For time dependent straining, two mechanisms will be considered: strain hardening attributed to the primary creep straining and material softening, or damage, due to creep constrained cavity nucleation and growth. The model also includes the effects of variable ductility with stress level, and the multi-axial stress state sensitivity of creep rupture. The influence of carbide coarsening on creep behaviour in 316 stainless steel has been studied by Dyson [12]. The conclusion is that the Ostwald-Ripening equation can

be used to assess the effect of carbide coarsening; and that below 550 °C, there should be no measurable effect of thermal exposure for up to 50 000 h. It can be seen from Fig. 4 that only one of the selected tests ($\sigma = 170$ MPa and $t_f = 102\,320$ h) has lifetime longer than 50 000 h. Particle coarsening effects have not been considered in the present CDM-based model.

The form of the constitutive equations for 316 stainless steel under uni-axial conditions is given by following equations set

$$\frac{d\varepsilon}{dt} = \frac{A}{(1-\omega_2)^n}\sinh(B\sigma(1-H)), \tag{5a}$$

$$\frac{dH}{dt} = \frac{h}{\sigma}\left(1 - \frac{H}{H^*}\right)\frac{d\varepsilon}{dt}, \tag{5b}$$

$$\frac{d\omega_2}{dt} = D\frac{d\varepsilon}{dt}, \tag{5c}$$

where σ and ε are uni-axial stress and strain, A, B, h, H^* and D are material constants, and the index n is given by $n = B\sigma(1-H)\coth(B\sigma(1-H))$, which is determined from the n-power stress dependence which is equivalent to the hyperbolic-sine stress dependence given by Eq. (5a). The state variable H is used to describe the strain hardening in the primary creep and the damage variable ω_2 describes grain boundary creep cavitation.

6. Procedure for fitting data to the model at high stress

The available test data obtained from constant load tests include initial loading strain, ε^{init}, and time independent plastic strain, ε^{tip}, which accumulates during creep tests. In order to obtain pure creep strains, ε, which are to be used to obtain material constants in the creep constitutive equations set (5), it is necessary to remove the time independent strains using the stress–strain curve discussed in Section 3.

To separate the creep strain from the total true strain, ε^t, it is necessary to recognise a total of three contributions:

1. Time independent initial plastic strains, ε^{init}, given directly by test data for the higher stress levels; and, by Eq. (1) for the lower stress levels.
2. Time independent plastic straining, ε^{tip}, which accumulates during the constant load creep test, due to stress increases resulting from finite deformations. These may be determined from Fig. 2 or Eq. (3). The subsequent levels of time independent straining are then determined from a modified stress–strain curve, c.f. Fig. 3, for 5% pre-strain.
3. The time dependent creep strain which is to be obtained using constitutive equations set (5).

The evaluation of contribution (i) has been carried out directly; contribution (ii) has been determined using a time incremental procedure involving approximately 500 time increments per creep test. Over each time increment, Δt, the increment of experimentally measured total strain, $\Delta\varepsilon^t$, has been obtained and the associated true stress change, $\Delta\sigma$, has been evaluated. Then, the corresponding time independent plastic strain, $\Delta\varepsilon^{tip}$, has also been determined using Eq. (3). In this way the increment of pure creep strain, $\Delta\varepsilon(= \Delta\varepsilon^t - \Delta\varepsilon^{tip})$, and the true stress have been evaluated for each interval. Since the increments of time independent plastic strain, $\Delta\varepsilon^{tip}$, have been calculated in very small increments of stress, $\Delta\sigma$, the simple additive decomposition of incremental strains ($\Delta\varepsilon = \Delta\varepsilon^t - \Delta\varepsilon^{tip}$) has been assumed to be valid and therefore has been used.

In the following sections, all the creep strain data discussed are pure creep strain data if not specified; and, stresses are true stresses obtained using the time independent strain–stress and creep strain-time curves.

6.1. Secondary creep at high stress

In creep tests, a region of steady state creep always exists called secondary creep. During this state, the creep rate is, in theory, constant under constant stress and is called minimum creep strain rate. In the uni-axial form of CDM-based constitutive equations set (6), the minimum creep strain rate is described by the material constants A and B; hence, parameters A and B can be determined from the available experimental minimum creep strain rate values.

To obtain A and B, it is assumed that $\omega_2 = 0$ and $H = H^*$ at the beginning of the secondary creep state. So Eq. (5a) becomes

$$\dot{\varepsilon}_{min} = A\sinh(B^*\sigma) = A(e^{B^*\sigma} - e^{-B^*\sigma})/2, \tag{6}$$

where $\dot{\varepsilon}_{min}$ is the minimum creep strain rate and $B^* = B(1-H^*)$. Furthermore, $e^{-B^*\sigma}/e^{B^*\sigma}$ tends to zero when $B^*\sigma \geq 1.5$, which is the condition usually met in practice. Then Eq. (6) becomes

$$\dot{\varepsilon}_{min} = A(e^{B^*\sigma})/2, \tag{7}$$

or in logarithmic form:

$$\ln(\dot{\varepsilon}_{min}) = \ln(A/2) + B^*\sigma. \tag{8}$$

The experimental minimum creep rates, $\dot{\varepsilon}^{(i)}_{min}$, where $i = 1, \ldots, m$ are the number of available test data, can be used to obtain approximate values of A and B^* as follows

$$A = \sum_{i=1}^{m-1} A^{(i)}/(m-1), \tag{9a}$$

$$B^* = \sum_{i=1}^{m-1} B^{*(i)}/(m-1), \tag{9b}$$

where

$$A^{(i)} = 2\exp(\ln\dot{\varepsilon}^{(i)}_{min} - B^{*(i)}\sigma^{(i)}), \tag{10a}$$

$$B^{*(i)} = (\ln \dot{\varepsilon}_{\min}^{(i)} - \ln \dot{\varepsilon}_{\min}^{(i+1)})/(\sigma^{(i)} - \sigma^{(i+1)}). \quad (10b)$$

More accurate values of the constants A and B^* can be obtained from the minimisation of the following error functional:

$$\phi_2 = \sum_{i=1}^{m} (\dot{\varepsilon}_{\min}^{\text{the}} - \dot{\varepsilon}_{\min}^{\text{exp}})^2, \quad (11)$$

where $\dot{\varepsilon}_{\min}^{\text{the}}$ and $\dot{\varepsilon}_{\min}^{\text{exp}}$ are theoretical or predicted and experimental minimum creep strain rates, respectively. For the optimisation scheme, the theoretical or predicted minimum creep strain rates, $\dot{\varepsilon}_{\min}^{\text{the}}$, have been obtained using Eq. (6) and the initial or starting values for A and B^* have been obtained from Eqs. (9a) and (9b).

6.2. Primary creep at high stress

The primary creep behaviour is described by material constants h and H^*. To obtain the values of h and H^*, a numerical optimisation technique, developed by Kowalewski et al. [14], has been used. The technique involves the digitisation of a series of points on the primary creep curves, and the use of equations set (5), with the current values of the material constants and assuming $\omega_2 = 0$, to predict the levels of strain at the times at which the points have been chosen. The square of error between predicted and experimental or digitised values of the primary creep strain at each individual point are then added over all creep curves to form the following error functional

$$\phi_3 = \sum_{i=1}^{M_H} \left\{ \sum_{j=1}^{a_i} (\varepsilon_j^{\text{the}} - \varepsilon_j^{\text{exp}})^2 \right\}_i, \quad (12)$$

where M_H is the number of creep curves at high stress, a_i is the number of points on the primary part of creep curve i, ε^{the} and ε^{exp} are the theoretical and experimental values of creep strain, respectively. The theoretical values for creep strains, ε^{the}, have been obtained using the constitutive equations set (5).

6.3. Complete creep curve at high stress

As discussed above, with the assumption of $\omega_2 = 0$ in primary and secondary creep state, material constants A and B have been obtained by using minimum creep rates; and, constants h and H^* by using primary creep curves. At this final stage, the optimisation problem will be defined in terms of creep strain and lifetime over the entire creep curves. The optimisation functional, which is similar to that in Eq. (12), is

$$\phi_4 = \sum_{i=1}^{M_H} \left\{ \left[\sum_{j=1}^{b_i} (\varepsilon_j^{\text{the}} - \varepsilon_j^{\text{exp}})^2 \right]_i + Z_i (t_i^{\text{the}} - t_i^{\text{exp}})/t_i^{\text{exp}} \right\}, \quad (13)$$

where M_H is the number of creep curves at high stress level, b_i is the number of points on curve i, ε^{the} and ε^{exp} are the predicted and experimental values of creep strains; and, t^{the} and t^{exp} denote predicted and experimental lifetimes, respectively. The term Z_i takes the values of Z_{il}, which is close to zero, when $t_i^{\text{the}} \le t_i^{\text{exp}}$; and, Z_{ih}, which is close to unity, when $t_i^{\text{the}} > t_i^{\text{exp}}$. In this way, the predicted results will remain in the lower or non-conservative bound. The last term of Eq. (13) has been normalised by dividing the error in lifetimes with experimental lifetime. In this way, firstly, the lifetime error term becomes dimensionless; and, secondly, its order of magnitude reduces to the same order as creep strain-error term.

The material constants D_i for each creep curve have been determined from the ductility relationship $D_i = 1/3\varepsilon_{\text{f}i}$, where $\varepsilon_{\text{f}i}$ is the rupture strain for curve i. This relationship can be obtained by integration of Eq. (5c) between initial and final values of $\omega_2 = 0$ at $\varepsilon = 0$; and, $\omega_{2\text{f}} = 1/3$ at $\varepsilon = \varepsilon_{\text{f}}$ [15]. At high stress levels, the values for creep strain at failure, ε_{f}, have been obtained using the experimental data. The starting values of A, B, h and H^* have been set to those previously determined. During the optimisation procedure, the variation of true stress with total strain, ε^{t}, has been obtained according to the relationship $\sigma = \sigma_0(1 + \varepsilon^{\text{t}})$. The required final material constants A, B, h and H^* have been obtained when a global optimum of the functional ϕ_4 has been achieved.

7. Procedure for fitting data to model high and low stress datasets together

7.1. Treatment of primary creep at low stress

For the experimental data at low stress, the loading data are not available. In order to remove the initial loading strain from the total strain curve, an estimated loading strain has been obtained using the power-law plasticity theory discussed in Section 3. However, the resulting creep curves show unexpected high primary creep. When the formulation proposed by Spindler [11] is adopted for the loading strain, the results are almost the same. Clearly, the available primary creep data at low stress are inconsistent, and therefore, in the absence of more precise information, the primary creep model used at high stresses has been adopted for creep at low stress levels.

7.2. Treatment of minimum creep rates and lifetimes

The data for minimum creep rates and lifetimes are readily available, and are not strongly dependent on initial loading strain. Furthermore, the important secondary creep stage is mainly described by the minimum creep rates and the lifetime. However, there are only a few data points available, as discussed above, on each experimental curve at low stress. In order to predict reasonable minimum creep

rates and lifetimes at low stress using the CDM model, a new relationship has been added to the optimisation functional equation (13). This new term includes the sum of the differences between the theoretical and experimental minimum creep rates and lifetimes. The resulting optimisation functional is

$$\phi_5 = \phi_4 + \sum_{i=1}^{q} \{\alpha_i(\dot{\varepsilon}_{\min}^{\text{the}} - \dot{\varepsilon}_{\min}^{\text{exp}})/\dot{\varepsilon}_{\min}^{\text{exp}} + \beta_i(t_i^{\text{the}} - t_i^{\text{exp}})/t_i^{\text{exp}}\}, \tag{14}$$

where ϕ_4 is the functional defined in Eq. (13), q is the number of available data at low stress, $\dot{\varepsilon}_{\min}^{\text{the}}$ and $\dot{\varepsilon}_{\min}^{\text{exp}}$ are theoretical and experimental minimum creep strain rates at low stress, t^{the} and t^{exp} are predicted and experimental lifetimes at low stress, and α_i and β_i are amplification factors. The amplification factors α_i and β_i take the values close to zero, when $t_i^{\text{the}} \le t_i^{\text{exp}}$; and, close to unity, when $t_i^{\text{the}} > t_i^{\text{exp}}$. In this way, the predicted results will remain in the lower or non-conservative bound. The experimental minimum creep rate and lifetimes at low stress are given in Table 4.

7.3. Creep rupture strains at low stress

The procedure to obtain the experimental failure creep strain in low stress tests is the same as for the high stress tests (Section 6) except that the initial time independent plastic strains are not available for the former tests. Hence, the initial strains have been obtained using the power-law model (Section 3). It has been found that the experimental creep rupture strains take unexpected high values when the stresses decrease. The possible reason for this have been explained by Dyson [12] who has taken into account the effect of the time independent plastic deformation in calculating lifetimes. In addition, the calculated initial loading strain may be different from the real values due to the cast dependency of the material behaviour.

Unlike thef high stress level, the use of experimental creep rupture strains, ε_f, to obtain the constitutive parameter, $D(=\omega_{2f}/\varepsilon_f)$, cause erroneous output in the optimisation procedure at low stress. In order to achieve the objective of this study, namely to predict reasonable results for the reheat cracking of pressure vessels, the predicted strains at failure under low stress level should be compatible with those of the in-plant service material, which are believed to be much lower than those measured in uni-axial tests. Furthermore, the rupture strain at high stress, addressed in the previous section, have also been taken into consideration. To obtain consistent values for the rupture strains, ε_f, the constitutive parameter, $D(=\omega_{2f}/\varepsilon_f)$, has been regarded as a variable in the optimisation functional at low stress level. In this way, the parameter D; and, consequently the strain at failure, ε_f, have been obtained from the minimisation of the optimisation functional ϕ at low stress level. It should be re-emphasised that, unlike the low stress level, at high stress level, the creep rupture strains have been obtained directly using the available experimental data (Section 6).

Finally, three rupture strains have been obtained for the three representative creep curves at low stress level. To obtain the final value for the rupture strains at low stress, small adjustments have been made within the bounds of scatter of the experimental data.

The optimisation technique which includes the high and low stress datasets will now be discussed.

Table 4
Minimum creep rate and lifetime at low stress

Initial stress (MPa)	232	201	170
Creep rates (%h^{-1})	2.556×10^{-4}	1.012×10^{-4}	3.983×10^{-5}
Lifetime (h)	15 043	41 057	102 320

7.4. Numerical optimisation procedure for fitting data at high and low stresses

To obtain material constants for the creep constitutive model for high and low stresses, firstly, the optimisation techniques discussed in the previous section has been used to obtain material constants for the creep model at high stress only. Then, a different approach has been adopted to extend the model to low stresses. In this approach, it has been assumed that the model for primary creep at high stress is valid at low stress as well. Hence, the material constants h and H^* will be the same for low and high stress levels. To include the effect of minimum creep strain rates and lifetimes at low stress, the associated error terms have been added into Eq. (13) to yield a new optimisation functional as follows

$$\phi_6 = \sum_{i=1}^{M} \left\{ \left[\sum_{j=1}^{a_i} (\varepsilon_j^{\text{the}} - \varepsilon_j^{\text{exp}})^2 \right]_i + Z_i\{(t^{\text{the}} - t^{\text{exp}})/t^{\text{exp}}\}_i + \alpha_i\{(\dot{\varepsilon}_{\min}^{\text{the}} - \dot{\varepsilon}_{\min}^{\text{exp}})/\dot{\varepsilon}_{\min}^{\text{exp}}\}_i \right\}, \tag{15}$$

where M is the total number of creep curves at low and high stress levels. Other parameters in Eq. (15) take the same values as those given in the previous sections.

In the optimisation procedure, material constants D_i for high stress and low stress test have been treated differently. For high stress level, D_i for each creep curve has been defined using the relationship $D_i = 1/3\varepsilon_{fi}$ while the rupture strains, ε_{fi}, have been obtained using the experimental data (Sections 4 and 6). For low stress creep curves, D_i has been regarded as an independent variable in the optimisation functional. Hence, the value of D_i and consequently creep rupture strain, ε_{fi}, have been obtained from the optimisation process for the low stress creep curves. The values of A, B, h

Table 5
Material parameters for the CDM-based creep constitutive equations set (5)

A (h)$^{-1}$	B (MPa)$^{-1}$	H (MPa)	H^*
0.2044×10^{-6}	0.1855×10^{-1}	0.4285×10^{5}	0.5113

and H^* which have been obtained from the optimisation process at high stress level are taken as the starting values for the final optimisation. The final values of material constants have been obtained when a global minimum value of ϕ_6 had been reached.

Finally, a fine adjustment has been made by regarding A, B, h and H^* as constant values and taking D_i as variables. The rupture strains are then adjusted according to the resulting D_i and the process is repeated, several times, until a convergent and satisfactory result has been achieved.

7.5. Summary of results for high and low stresses

The final material constants are given in Table 5 and the optimisation results are given in Figs. 7 and 8 for high and low stress levels, respectively. In both figures the definition of stress and strain are the initial engineering stress and pure creep strain, respectively. Symbols denote the experimental results and the solid lines denote the predicted creep strain.

From Fig. 7, it is clear that the agreement between experimental data and the predicted values at high stress is very good. Fig. 8 shows the comparison between the experimental data and predicted values at low stress. As expected, it can be seen that the agreement between experimental and predicted values of minimum creep rates and of lifetimes are good. However, the experimental creep curves at low stress show high primary creep.

The experimental and predicted creep properties are shown in Figs. 9–12. It is worth recalling that these figures, unlike Figs. 4–6, show the pure creep properties. In other words, the accumulated time independent creep strain, ε^{tip}, has been separated from pure creep strain. Also in these

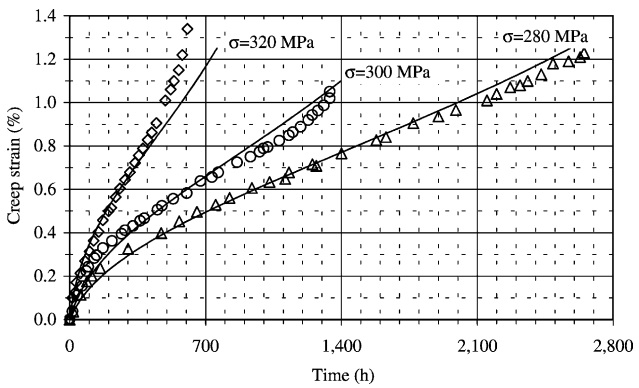

Fig. 7. Variation of the creep strain with time for the selected high stress tests. The symbols denote the experimental results and the solid lines denote the theoretical predictions. Stresses are initial engineering stress.

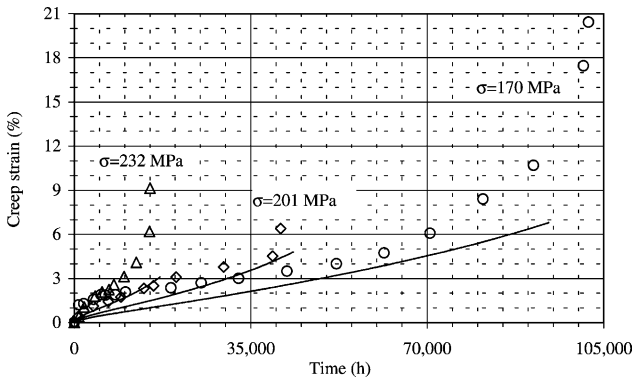

Fig. 8. Variation of the creep strain with time for the selected low stress tests. The symbols denote the experimental results and the solid lines denote the theoretical predictions. Stresses are initial engineering stress.

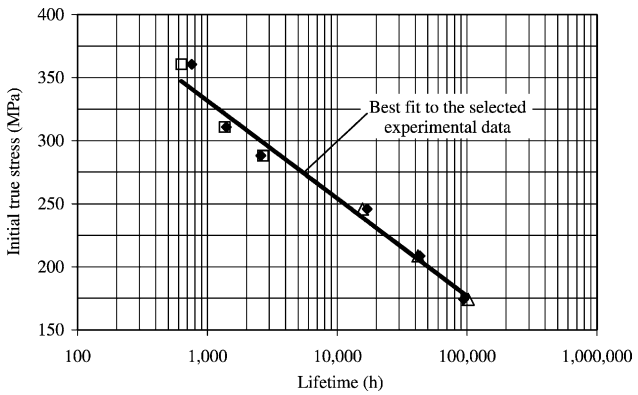

Fig. 9. Variation of the lifetime with initial true stress for uni-axial creep data for AISI 316 at 550 °C. The solid diamonds denote the predicted results. The square and triangular symbols denote the selected test results for high stress and low stress levels, respectively, which have been chosen using Fig. 4. The solid line is the best fit to the selected experimental data.

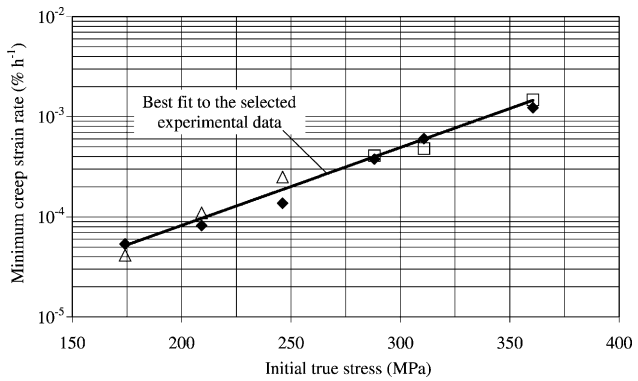

Fig. 10. Variation of the minimum creep strain rate with initial true stress for uni-axial creep data for AISI 316 at 550 °C. The solid diamonds denote the predicted results. The square and triangular symbols denote the selected test results for high stress and low stress levels, respectively, which have been chosen using Fig. 4. The solid line is the best fit to the selected experimental data.

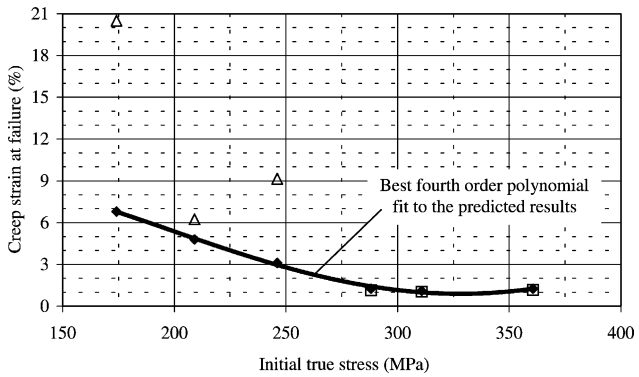

Fig. 11. Variation of the creep strain at failure with initial true stress for uni-axial creep data for AISI 316 at 550 °C. The solid diamonds denote the predicted results. The square and triangular symbols denote the selected test results for high stress and low stress levels, respectively. The solid line is the best fourth order polynomial fit to the predicted/empirical results and represents the empirical data to be used in the proposed model.

figures, the definition of the initial true stress is given by

$$\sigma^{\text{init.true}} = \sigma^{\text{init.eng}}(1 + \varepsilon^{\text{init.eng}}), \tag{16}$$

where the initial true stress, $\sigma^{\text{init.true}}$, is the applied constant load divided by the current cross-sectional area of the testpiece, after initial time independent plastic straining. For the high stress level tests, initial engineering strain, $\varepsilon^{\text{init.eng}}$, has been determined directly from recorded test data, and for the low stress levels, $\varepsilon^{\text{init.eng}}$ has been determined using power-law equation (1), since no test data was available. Fig. 9 shows the variation of the lifetime with initial true stress. The solid diamonds denote the predicted results and the square and triangular symbols denote the selected test results for high and low stress levels, respectively. Fig. 9 shows that the agreement between the selected experimental data and the predicted results is excellent, and that they are all very close to the solid line which provides a best least square fit to the selected experimental data. This figure also shows a linear

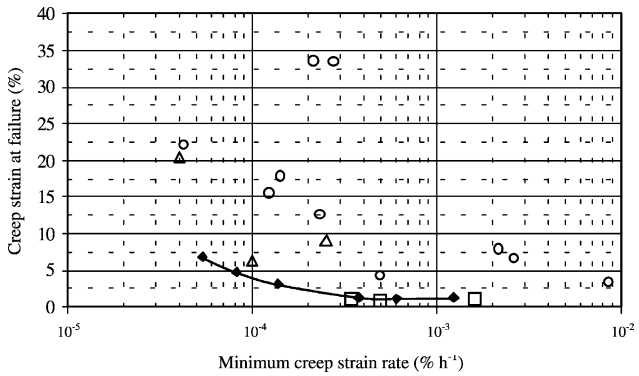

Fig. 12. Variation of the creep strain at failure with minimum creep strain rate. The open circles denote the average of the experimentally measured values for all test data at 550 °C. The square and triangular symbols denote the selected test results for high stress and low stress levels, respectively. The solid diamonds denote the predicted results. The solid line is the representation of the fourth order polynomial fit to the predicted values shown in Fig. 11.

relationship between initial true stress and logarithm of lifetime. The minimum creep strain rates against initial true stress are presented in Fig. 10. The solid diamonds denote the predicted results and the square and triangular symbols denote the selected experimental results for high and low stress levels, respectively. The solid line denotes the best least square fit to the selected experimental points. It can be seen that the predicted minimum creep strain rates agree very well with the selected experimental results except at an initial true stress level of $\sigma^{\text{init.true}} = 248$ MPa. The figure shows that all the predicted results (diamond symbols) are close to the solid line least square fit to the experimental points. Also the figure indicates a linear relationship between initial true stress and logarithm of minimum creep strain rate. The predicted results, presented in Figs. 9 and 10, do not fall exactly along the solid line due to the variation in creep ductility obtained during the fitting of individual creep curves.

The creep rupture strains are shown in Fig. 11. In this figure, the solid diamonds denote the predicted results and the square and triangular symbols denote the selected test results for high and low stress levels, respectively. The solid line denotes the best fourth order polynomial fit to the predicted/empirical results. From Fig. 11, it can be seen that the predicted low stress creep rupture strains are a lower bound to the experimental values; and that for the high stress levels the predicted and the experimental values are in close agreement. The reason for this is that the rupture creep strains for high stress levels, shown by rectangular symbols, are obtained using the available experimental data (Section 6). However, at low stress levels, the creep rupture strains, shown by triangular symbols, have been obtained using the procedure discussed in Section 7.3 which yields unexpectedly high values. It has been recognised that the predicted strains at failure under low stress level should be compatible with those of the material in plant service, which is believed to be much lower than those measured in uni-axial tests [12]. The rupture strains predicted by the solid line in Fig. 11 is to be used in the proposed model which allows the creep rupture strains to change with stress. Therefore, the CDM-based model will provide a non-conservative results in terms of reheat crack initiation and growth.

Fig. 12 shows the variation of the experimentally measured creep strains at failure with minimum creep strain rate. The open circles denote the average values of the experimentally measured rupture strains for all Type 316 and 316H casts at 550 °C. The square and triangular symbols denote the selected test results for high stress and low stress levels, respectively. The solid diamonds denote the predicted results using the CDM-based model. The solid line is the representation of the fourth order polynomial fit to the predicted results shown in Fig. 11. In Fig. 12, all the data points denote pure creep rupture strain, except the open circles which denote the average values of the experimentally measured rupture strains at a particular stress level. In other words, the latter data points include

the time independent plastic strain, ε^{tip}, which accumulates during the constant load creep tests. Fig. 12 shows

1. There is a very wide scattered band for creep test data [7–9]. The figure shows a range of values of 3.5–22.2% for the average values of creep rupture strains for all Type 316 and 316H casts at 550 °C. Possible reasons for this are heat treatment, pre-straining [12] and different casts of material [11].
2. The selected single test points, represented by the triangular and rectangular symbols follow the lower bound pattern shown by the open circles which denote average experimental values.
3. The predicted results, denoted by the solid diamonds, and the solid line, in Figs. 11 and 12 represent a non-conservative bound for the rupture strains.

8. Conclusion

A model has been developed to describe the time independent and time dependent straining of AISI 316 stainless steel at 550 °C. The materials dataset has been selected for its relation with the Haysham I superheater header; and, hence the CDM-based constitutive equations can be used in subsequent reheat cracking studies of that vessel. The procedure adopted in this paper is not intended to be a general procedure for the development of CDM-based models to describe combined time independent plasticity and time dependent creep. However, it outlines a method which has been specifically developed and used to fit a dataset which contains significant scatter. Despite the paucity of experimental data at low stress levels, the model has been shown to predict the results of uni-axial experiments over a very wide stress range, with some deficiencies at lower stress levels.

More accurate creep data is required at low stress, particularly for initial loading strains, primary creep strains, and for creep ductility. It is only then that the precision of creep model can be improved.

The model has been shown to be suitable for use in finite element modelling studies of reheat cracking in operational plant welded from AISI 316 stainless steel.

Acknowledgements

The results of this research have been obtained through funding provided by the HSE, IMC programme, which the authors gratefully acknowledge. Interactions with the staff of British Energy Generation Ltd, Barnwood, during the course of the research, have been invaluable. Acknowledgment for permission to publish the long term creep test results is given to the sponsors of the ERA Technology Project-4080 from which the low stress data originate, in particular ALSTOM Power (UK) Ltd, British Energy plc; and, PowerGen plc.

References

[1] Holt PJ. Heysham I/ Hartlepool superheater header weld S4. Revised finite element residual stress and reheat cracking analysis. British Energy Report No. EDP/AGR/REP/0326/97, Issue 1, British Energy Generation Ltd; 1997.
[2] Bradford RAW. Finite element modelling of reheat cracking initiation in austenitic weldments. Proc Int Conf Assuring It's Safe, IMechE 1998.
[3] Hayhurst DR, Brown PR, Morrison CJ. The role of continuum damage in creep crack growth. Phil Trans R Soc, Lond, A 1984;311:131–58.
[4] Hayhurst DR, Dyson BF, Lin J. Breakdown of the skeletal stress technique for lifetime prediction of notched tensions bars due to creep crack growth. Engng Fract Mech 1994;49:711–26.
[5] Hall FR, Hayhurst DR, Brown PR. Prediction of plane-strain creep crack growth using continuum damage mechanics. Int J Damage Mech 1996;5:353–83.
[6] Vakili-Tahami F, Hayhurst DR. Initiation, growth of damage and subsequent creep crack growth due to reheat cracking of A 316H stainless steel welded pressure vessel at 550 °C. Internal Research Report DMM.01.05, Third issue, 19th October 2001. Mech. Aerospace and Manufacturing Engineering, UMIST; 2001.
[7] Grover HK, Higginbottom A. Final report on the elevated temperature tensile and creep properties of Type 316 steel. ERA Report 2A/858; 1983.
[8] Hutchings D. Creep testing of specimens from ex-Heysham superheater outlet header 1B2/4. British Energy Report TEL/MEM/0204/94, Issue 1, British Energy Generation Ltd; 1994.
[9] Kimmins ST. Materials data for use in the structural integrity assessments of Heysham I/Hartlepool superheater outlet headers. British Energy Report ED/HYA/REP/0153/95, British Energy Generation Ltd; 1995.
[10] British Standards Institution. Guidance on methodology for assessment of stress-rupture data. Procedure for derivation of strength values, BS PD6605-1; 1998.
[11] Spindler MW. Creep ductility of Type 316 and 316H austenitic stainless steels between 500 and 700 °C. British Energy Report EPD/AGR/REP/0051/96, Issue 1, British Energy Generation Ltd; 1996.
[12] Dyson BF. An alternative constitutive description of AISI 316 stainless steel for use in weld re-heat cracking. Internal Research Report, British Energy plc, Barnwood, Gloucester; 1997.
[13] Henderson J, Harwood N, Rooney D. Creep characterisation of a Type 316 austentic steel. High Temp Technol 1987;5(4):181–92.
[14] Kowalewski ZL, Hayhurst DR, Dyson BF. Mechanisms-based creep constitutive equations for aluminium alloy. J Strain Anal 1993;29(4):309–16.
[15] Dyson BF, Gibbons TB. Tertiary creep in nickel-based superalloys: analysis of experimental data and theoretical synergies. Acta Metall 1987;35(9):2355–69.